

# ATR-FTIR AND THERMAL BEHAVIOR STUDIES OF NEW HYDROGEL FORMULATIONS BASED ON HYDROXYPROPYL METHYLCELLULOSE/POLY(ACRILIC ACID) POLYMERIC BLENDS

MIRELA-FERNANDA ZALTARIOV, DANIELA FILIP,  
CRISTIAN-DRAGOS VARGANICI and DOINA MACOCINSCHI

“Petru Poni” Institute of Macromolecular Chemistry, 41A, Gr. Ghica-Voda Alley,  
700487, Iasi, Romania

✉ Corresponding author: M.-F. Zaltariov, zaltariov.mirela@icmpp.ro

*Dedicated to the 70<sup>th</sup> anniversary of  
Acad. Bogdan C. Simionescu*

Stimuli-responsive drug delivery polymeric systems based on physical interactions between all the components: Hydroxypropyl methylcellulose (HPMC) and Poly(acrylic acid) (PAA) loaded with anise/fluconazole  $\beta$ -cyclodextrin (FCZ- $\beta$ -CD) inclusion complexes, in 1:2 and 1:3 ratios, were prepared and characterized by temperature-dependent ATR-FTIR spectroscopy, DSC and TGA analyses. The successful embedding of the FCZ- $\beta$ -CD inclusion complex into polymeric matrices was evidenced by IR spectroscopy and DSC data. The H-bonding interactions between HPMC and PAA were found to be stronger by increasing the HPMC content in the gel formulations, while  $E_H$  varied from 21.29 kJ to 25.89 kJ. The DSC thermograms and TG/DTG curves revealed several endotherms and multiple degradation stages, respectively, because the studied hydrogels were multicomponent systems with complex interactions among all the constituents.

**Keywords:** hydroxypropyl methylcellulose, fluconazole  $\beta$ -cyclodextrin inclusion complex, ATR-FTIR, thermogravimetric analysis

## INTRODUCTION

Cellulose derivatives are rapidly becoming a promising and important class of materials, an important trend of the scientific world directed toward green and environmentally friendly resources. Over the last few years, the research has been focused on improving the chemical and physical properties of cellulose.

The properties of polymeric materials can be improved by chemical modification, by physical interactions between all the components, or by polymer blending, resulting in innovative architectures. Chemically modified cellulose derivatives obtained by graft copolymerization techniques have attracted special attention, since they allow the introduction of the desired functionality to natural polymers.<sup>1</sup> Interpolymer complexes or polymer blending approaches have also received particular attention during the last

years. Different complex formations by using hydrogen bonding have been reported between polyacrylic acid and poly(vinyl ether) or diethylene glycol and cellulose.<sup>2</sup> Several studies have focused on the effect of temperature, solvent and physical crosslinking of HPMC/PAA blends on the drug release. H-bonding interactions were found to be stronger in blended formulations prepared from water than those prepared from water/ethanol mixture, mainly due to the formation of inter-associated hydrogen bonds.<sup>3</sup> By this approach, the compatibility of immiscible blends could be improved in order to modify the properties of the polymeric blends efficiently. Thus, the literature data reveal that poly(acrylic acid) forms miscible blends with polyethylene oxide (PEO), as does polyethylene glycol (PEG) with poly(1-vinylimidazole) or poly(2-methyl-5-

vinyl tetrazole).<sup>4</sup> Also, in methylcellulose/polyvinyl alcohol (PVA) blends, an interconnected polymeric network is formed based on the affinity of hydrogen bonds between the -OH groups of the C-2 or the C-3 position of cellulose and the side chain -OH groups of polyvinyl alcohol and those between the ring

oxygen (O-5) of cellulose and the -OH groups of the PVA (Fig. 1(a)).<sup>5</sup> Biocompatible and flexible blends with improved degradability properties have been obtained from hydroxypropyl cellulose (HPC), an alkyl-substituted hydrophilic cellulose derivative, and PVA.<sup>6</sup>

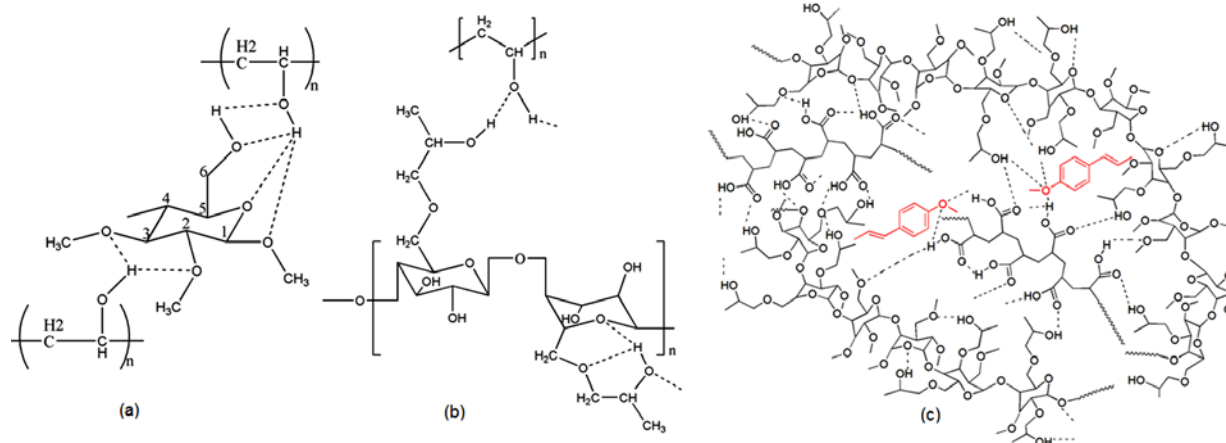


Figure 1: Schematic representations of intermolecular interactions in different blends based on: MC/PVA (a), HPMC/PVA (b) and HPMC/PAA (c)

Table 1  
Formulation of F1A and F2A bioadhesive gels with anise and fluconazole/ $\beta$ -cyclodextrin inclusion complex

Ingredients, g	F1A_1:2	F1A_1:3	F2A_1:2	F2A_1:3
Fluconazole	1	1	1	1
$\beta$ -cyclodextrin	2	3	2	3
PAA	0.1	0.1	0.1	0.1
HPMC	0.1	0.1	0.2	0.2
Poloxamer 407	1	1	1	1
DMSO (mL)	0.2	0.2	0.2	0.2
TEA	1	1	1	1
Glycerol	10	10	10	10
Aq. anise extract	19.4	19.4	19.4	19.4
Distilled water q.s.	80	80	80	80

A high swelling capacity, with significant effects on the kinetics of drug release, was found for the polymer blends based on HPMC, which is a water-soluble, non-toxic, low cost, biodegradable and biocompatible cellulose derivative, and is used in solid dispersion in numerous drugs (Fig. 1 (b)).<sup>7-11</sup>

The present paper is an extension of our previous work<sup>11</sup> and is focused especially on the effect of the crosslinking agent (PAA) and the anise/fluconazole  $\beta$ -cyclodextrin inclusion complex on the polymeric blending formation and stability. ATR-FTIR, DSC and TG/DTG studies between different ratios of HPMC, PAA and

anise/fluconazole  $\beta$ -cyclodextrin inclusion complex are presented and discussed.

## EXPERIMENTAL

### Materials

The aqueous anise oil extract (1% w/w anise oil) was obtained by the steam distillation procedure<sup>12</sup> from star anise seeds. Hydroxypropyl methylcellulose (Aldrich), triethanolamine (Aldrich), poly(acrylic acid) (Serva Fein Biochemica Heidelberg) and glycerol (Cremer Oleo, Germany) were used as received without purification. Hydrogel formulations (F1A-F4A), containing 0.15% w/w anise oil (A), were prepared by a previously described procedure.<sup>11</sup> The composition of the gel formulations with embedded

inclusion complexes of  $\beta$ -cyclodextrin with 1% wt/wt fluconazole in 1:2 and 1:3 ratios is presented in Table 1. These hydrogels were selected by their biocompatibility, considering the values of interfacial tension between blood and the film surface. For the selected samples, these values were as follows: 1.6 mN/m for F1A and 1.0 mN/m for F2A.<sup>11</sup>

## Methods

### Attenuated Total Reflectance Fourier Transform Infrared Spectroscopy (ATR-FTIR)

The infrared (IR) measurements were carried out on a Bruker Vertex 70 spectrometer (Bruker Optics, Ettlingen, Germany). The spectra were recorded in the ATR (Attenuated Total Reflectance) mode in the range of 4000–600  $\text{cm}^{-1}$  with a resolution of 4  $\text{cm}^{-1}$ , at room temperature.

The temperature-dependent ATR-FTIR spectra were recorded in both heating and cooling runs on the Bruker Vertex 70 FT-IR Instrument equipped with a Golden Gate single reflection ATR accessory and a temperature controller. The solid samples were added on the ATR crystal surface and sealed with a cap. The temperature was varied between 27 and 55  $^{\circ}\text{C}$ , with increases of 10  $^{\circ}\text{C}$  at each registration. After the temperature was changed, the sample was maintained 2 min before the acquisition of the spectrum. The registrations were performed in the ATR mode in the 600–4000  $\text{cm}^{-1}$  spectral range, with 64 scans and a resolution of 2  $\text{cm}^{-1}$ .

### Differential scanning calorimetry (DSC)

DSC measurements were performed on a DSC 200 F3 Maia device (Netzsch, Germany). Each 5 mg of sample was heated in aluminum crucibles with pierced and pressed lids. Heating/cooling rates of 10  $^{\circ}\text{C min}^{-1}$  were applied, operating under nitrogen flow, at the flow rate of 50  $\text{mL min}^{-1}$ . The device was calibrated with indium, according to standard procedures.

### Thermogravimetric analysis (TGA)

TGA thermograms were recorded on an STA 449 F1 Jupiter device (Netzsch, Germany). Approximately 10 mg of each sample was heated in an open alumina crucible under nitrogen flow, with the flow rate of 50  $\text{mL min}^{-1}$  and a heating rate of 10  $^{\circ}\text{C min}^{-1}$ . The samples were heated in the range of 30–700  $^{\circ}\text{C}$ .

## RESULTS AND DISCUSSION

### ATR-FTIR

FTIR spectroscopy is a very helpful method to study inter- and intramolecular interactions between particular macromolecular systems, where different complementary donor-acceptor groups are present. The occurrence of the hydroxyl groups in the structure of HPMC, acting as donor, and of the carboxylic groups in the structure of PAA, acting as donor to –OH groups

and as acceptor to carbonyl (C=O) groups, leads to the formation of a strong connected network through H bonds. A schematic representation of the intermolecular complexes created by physical interactions between the two macromolecular chains (HPMC and PAA) can be seen in Figure 1(c).

ATR-FTIR analysis of the samples revealed the most representative bands in the range of 3800–3000  $\text{cm}^{-1}$  assigned to –OH intra- and intermolecular stretching modes of the HPMC and PAA polymer mixtures (F1A–F4A).

The number and position of the peaks in the –OH spectral region were determined through the second derivative spectrum. The –OH spectral region was deconvoluted by the curve-fitting method and the areas were calculated by a 50% Lorentzian and 50% Gaussian function, using OPUS 6.5 software. The procedure led to the best fit of the original curve with an error of less than 0.001.

The H bonding distances were obtained using the Sederholm equation:<sup>13</sup>

$$\Delta\nu (\text{cm}^{-1}) = 4.43 \cdot 10^3 \cdot (2.84 - R) \quad (1)$$

where  $\Delta\nu = \nu - \nu_0$ ,  $\nu_0$  is the standard wavenumber corresponding to free O–H groups located at 3650  $\text{cm}^{-1}$ ,  $\nu$  is the stretching wavenumber of the H-bonded O–H groups in the IR spectra of the analyzed samples.

The energy of the H bonds ( $E_H$ ) was calculated by using the formula:<sup>14</sup>

$$E_H = \frac{1}{k} \frac{\nu_0 - \nu}{\nu_0} \quad (2)$$

where  $1/k$  is a constant equal to  $2.625 \cdot 10^2$  kJ.

The formation of strong intermolecular H-bonds between HPMC and PAA was evidenced from the shifts of the absorption bands characteristic of the hydroxyl groups in HPMC (3460  $\text{cm}^{-1}$ ) and PAA (3200  $\text{cm}^{-1}$ ) to lower wavenumbers (3354 and 3100  $\text{cm}^{-1}$ , respectively) (Fig. 2).

As a result of the strong interactions between HPMC and PAA, the band at 1703  $\text{cm}^{-1}$  assigned to the carbonyl group in the IR spectrum of PAA is blueshifted to 1659  $\text{cm}^{-1}$ . The H-bonding interactions between HPMC and PAA were found to be stronger with the increase in the HPMC content in the mixture,<sup>11</sup> while  $E_H$  varied from 21.29 kJ to 25.89 kJ. This behavior could be due to the complex interactions between the two polymer chains by combining inter- and intramolecular H bonding. This feature is highlighted by the presence of several vibrations

of the –OH groups in the deconvoluted IR spectra (Fig. 2) of the physical mixtures of polymers F1A-F4A, which are blueshifted upon increasing the HPMC content. Thus, the band at  $3450\text{ cm}^{-1}$  in F1A, assigned to the intramolecular interactions between the –OH groups and O-6 in HPMC,<sup>15-17</sup> is blueshifted to  $3430\text{ cm}^{-1}$  in F2A and to  $3412\text{ cm}^{-1}$  in F3A and F4A. The band at  $3354\text{ cm}^{-1}$ , attributed to –OH vibration, involved in the formation of the intermolecular interactions between the –OH groups of HPMC as donor and the carbonyl groups of PAA as acceptor, is blueshifted to  $3290\text{ cm}^{-1}$  upon increasing the HPMC content. The two absorption bands at  $3266\text{ cm}^{-1}$  and  $3188\text{ cm}^{-1}$  assigned to the intramolecular H-bonds, which occur between the –OH groups and the C-O-C groups in the structure of HPMC, are also blueshifted with  $20\text{-}40\text{ cm}^{-1}$  as the HPMC content is increased.<sup>16</sup> Finally, the band at about

$3100\text{ cm}^{-1}$  in the IR spectra of the polymeric mixtures is attributed to the –OH groups of PAA involved as donor in H bonding with oxygen atoms in the structure of HPMC.

Besides the broad band specific to the hydroxyl group vibrations, the ATR-FTIR spectra of the HPMC/PAA based hydrogels exhibited particular bands assigned to the singular chain structures: symmetric and asymmetric stretches of –C-H bonds at  $2943, 2922\text{ cm}^{-1}$  and  $2881, 2831\text{ cm}^{-1}$  respectively, stretching frequencies of the carbonyl group (C=O) at  $1659\text{-}1717\text{ cm}^{-1}$ , deformation vibration of the –CH<sub>2</sub>-CO- group at  $1449\text{ cm}^{-1}$ , –C-H bending at  $1354\text{ cm}^{-1}$ , –CH<sub>2</sub> wagging at  $1317\text{ cm}^{-1}$ , C-O stretching at  $1250\text{ cm}^{-1}$ , C-O-C stretching at  $1065\text{ cm}^{-1}$  and  $1034\text{ cm}^{-1}$ , ring asymmetric stretching at  $947\text{ cm}^{-1}$  (Fig. 3).<sup>18,19</sup>

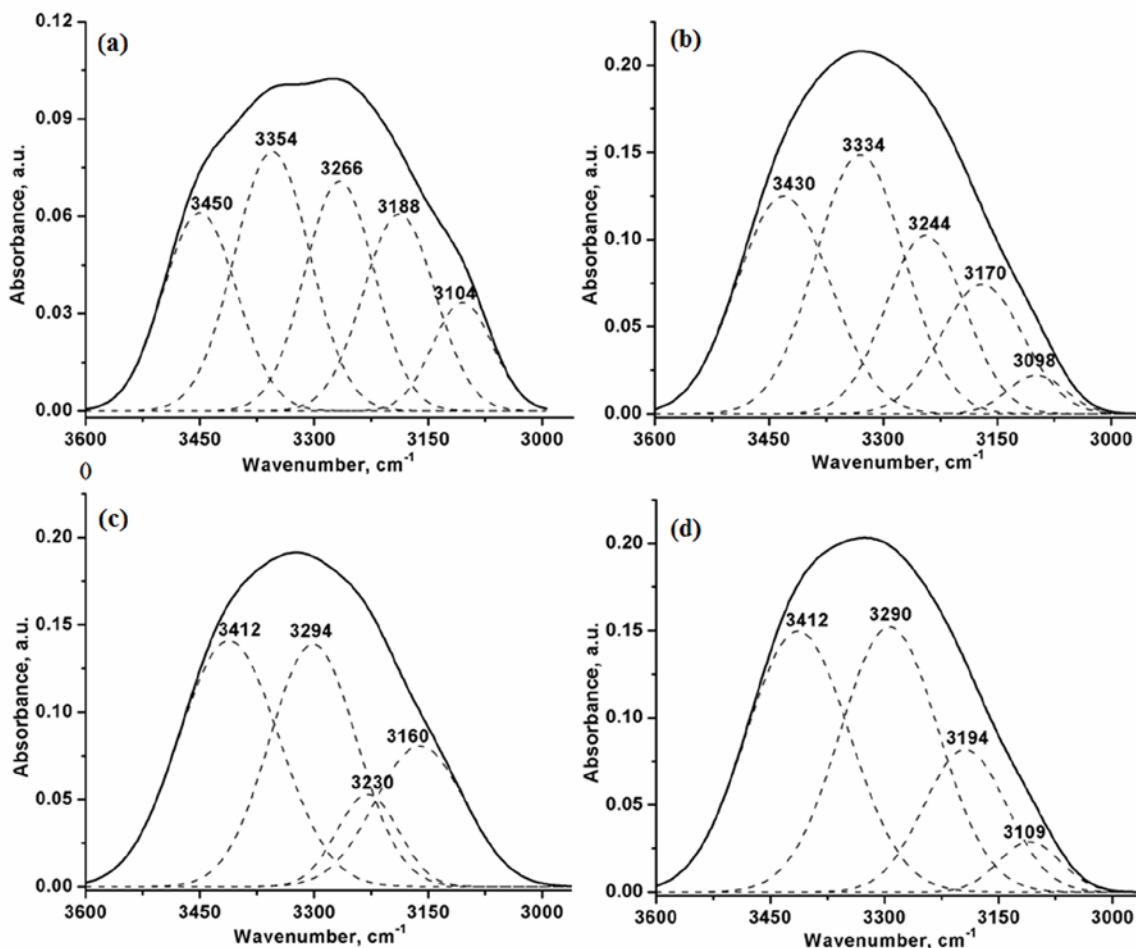


Figure 2: Deconvoluted IR spectra of PAA-HPMC based hydrogels in  $2960\text{-}3600\text{ cm}^{-1}$  spectral region: (a) F1A, (b) F2A, (c) F3A and (d) F4A

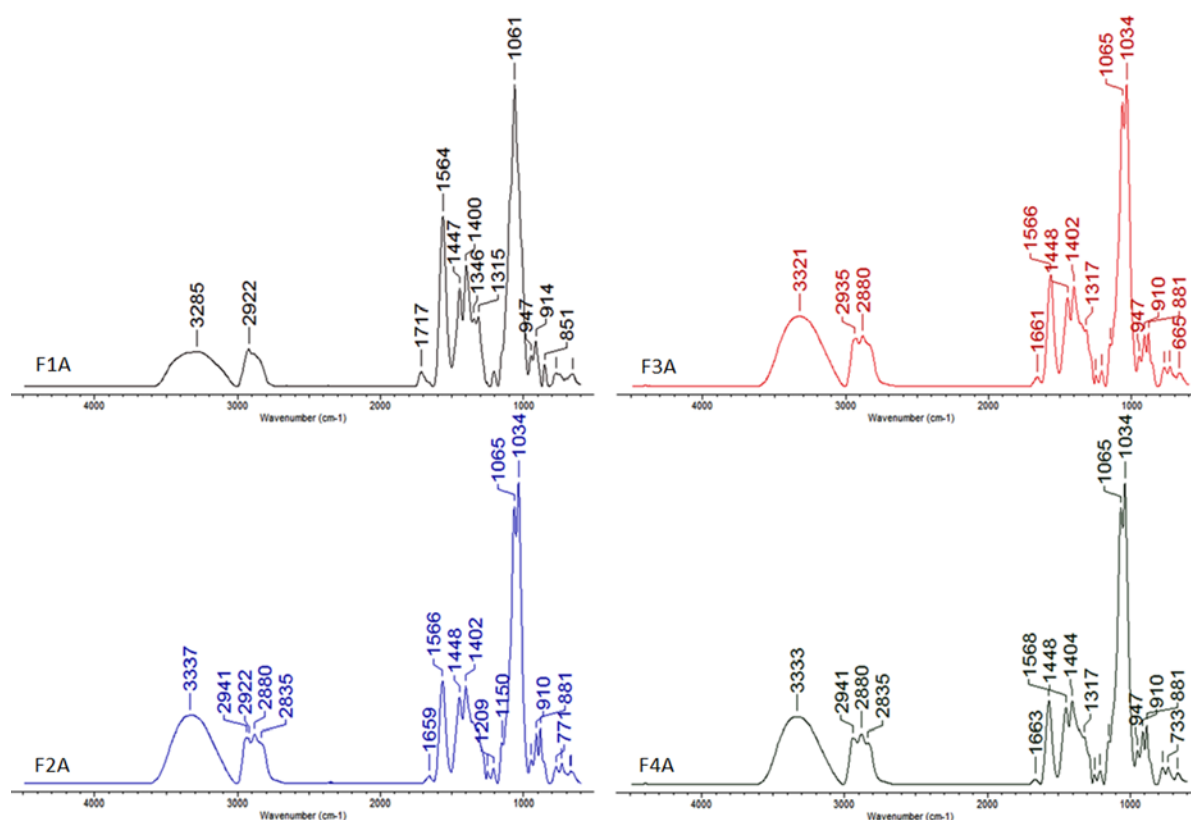


Figure 3: ATR-FTIR spectra of HPMC/PAA based hydrogels

Even if in these polymeric mixtures there is a greater number of OH groups, which contribute to the formation of a large number of intra- and intermolecular H bonds, the strength of the hydrogen bonded systems has been found to depend not only on the number of hydrogen bonds, but also strongly on the particular arrangement of the donor and acceptor functional groups. The structural flexibility of PAA with its participation in the formation of hydrogen bonds as both donor and acceptor is the main factor that could determine the formation of stronger interactions within the polymer networks.

Because of the dynamic character of the H-bonds, due to their weaker nature as compared to the covalent bonds, the supramolecular polymeric complexes are kinetically more labile, dynamically more flexible and thermodynamically less stable than classical covalent polymers.<sup>20,21</sup> To prove these characteristics, the studied hydrogels were investigated in the 27-55 °C temperature range by the FTIR spectrometer equipped with a temperature controller. The spectra were registered every ten degrees during the heating and cooling processes. As expected, as the

temperature increases, the H bonds are broken. The IR spectra reveal the absorptions characteristic of the -OH of the absorbed water vapor at 3724 cm<sup>-1</sup>,<sup>22</sup> broad and low intensity absorption bands in the range of 3400-3000 cm<sup>-1</sup>, assigned to the free -OH groups from HPMC and PAA, the vibrations specific to the carboxylic groups were redshifted with 30 cm<sup>-1</sup> and the broad bands in the 2700-2600 cm<sup>-1</sup> range attributed to the H bonds between the carboxylic groups ( $\text{R}-\text{C}(=\text{O})-\text{O}-\text{H}\cdots\text{O}-\text{C}(=\text{O})-\text{R}$  dimers) in the PAA polymeric chains (Fig. 4).

This behavior reveals a high affinity for hydrogen bond formation between the carboxyl groups, which could not be identified as free groups, but rather only in the dimer form in the IR spectra at higher temperature. Upon cooling, in the same temperature range, a reverse trend toward the re-formation of the H bonds can be seen. In the IR spectra registered during the cooling process, the characteristic absorptions of H-bonding are present, but the rate of H bond re-formation is lower than that of dissolution (Fig. 5). This may be explained by the fact that the strength of the association between the HPMC

and PAA polymeric chains is highly dependent on the assembly mechanism, their concentrations, temperature, the solvent used and the environmental factors involved in the initial mixtures.<sup>20,23</sup> The successful embedding of the  $\beta$ -CD-fluconazole complex into polymeric matrices F1A and F2A was first proved by IR spectroscopy. Thus, in the IR spectra of samples F1A and F2A, the characteristic absorptions of –

OH groups (from HPMC, PAA,  $\beta$ -CD, fluconazole) in the 2960-3600  $\text{cm}^{-1}$  spectral range (Fig. 6) overlapped with C-H stretches from the triazole ring at 3116  $\text{cm}^{-1}$ , with C=C and C=N stretches at 1620  $\text{cm}^{-1}$  and 1568-1570  $\text{cm}^{-1}$ , respectively.

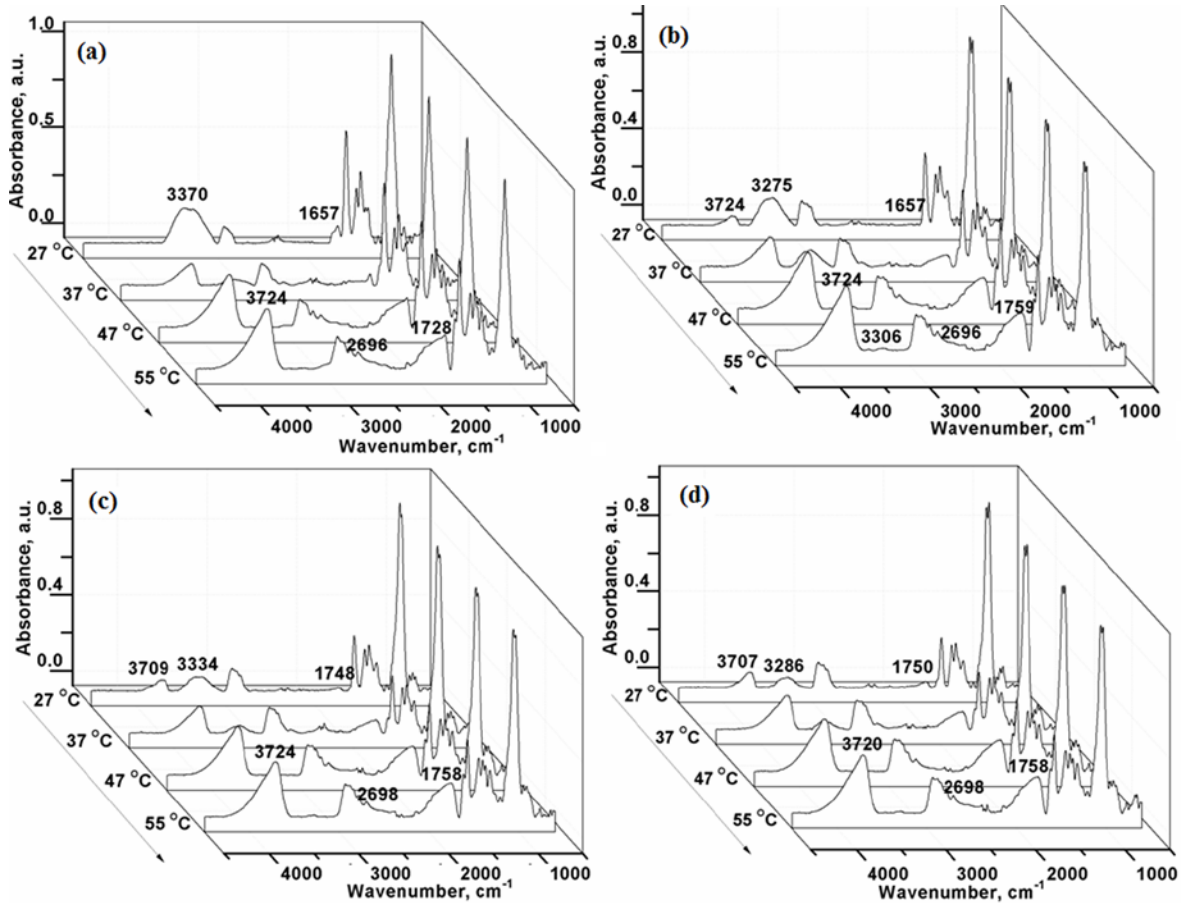


Figure 4: ATR-FTIR spectra of hydrogels F1A (a), F2A (b), F3A (c) and F4A (d) during heating from 27 to 55 °C

The ring stretch, overlapped with C-H bend vibrations, occurs at 1332  $\text{cm}^{-1}$  and 1252  $\text{cm}^{-1}$ , while the ring bend vibrations are observed at 1109  $\text{cm}^{-1}$  and 939  $\text{cm}^{-1}$ . The presence of the 2,4-difluorobenzyl groups in the structure of fluconazole is highlighted by the band at 755  $\text{cm}^{-1}$  and the band at 1273  $\text{cm}^{-1}$  assigned to the C-F stretches. Other specific bands are attributed to the C-O stretch at 1026  $\text{cm}^{-1}$ , overlapped with those from HPMC, to the  $\text{CH}_2$  scissor absorptions at 1450  $\text{cm}^{-1}$ , C-C stretches at 1145  $\text{cm}^{-1}$  and a combination of –OH bending,  $\text{CH}_2$  bending and  $\text{CH}_2$  deformation at 1410-1414  $\text{cm}^{-1}$  (Fig. 7).<sup>24-26</sup>

Even if, in the  $\beta$ -CD-fluconazole based HPMC-PAA polymeric mixtures, a greater number of –OH groups contribute to the formation of a large number of intra- and intermolecular H bonds, the strength of the hydrogen bonded systems has been found to be weaker, compared to the polymeric mixtures F1A and F2A, considering the  $E_H$  of hydrogen bonding –OH groups of HPMC (Table 2). The found values ranged between 19.13-19.41 kJ for F1A\_1:2 and F1A\_1:3, and between 18.55-19.99 kJ for F2A\_1:2 and F2A\_1:3, respectively.

However, the existence of strong polymeric networks based on HPMC/PAA and  $\beta$ -CD-fluconazole is due to the additional H bonds formed between the  $-\text{OH}$  groups (from HPMC, PAA,  $\beta$ -CD), as donors, and  $-\text{C}=\text{N}$  from the triazole ring in the fluconazole molecules, as acceptors. Thus, the bands at  $3444\text{--}3466\text{ cm}^{-1}$  in samples F1A\_1:2, F1A\_1:3, F2A\_1:2 and

F2A\_1:3 are specific to the intramolecular interactions between the  $-\text{OH}$  groups and O-6 in HPMC.<sup>15-17</sup> The absorptions at  $3384\text{ cm}^{-1}$  (F1A\_1:2),  $3380\text{ cm}^{-1}$  (F1A\_1:3),  $3372\text{ cm}^{-1}$  (F2A\_1:2) and  $3392\text{ cm}^{-1}$  (F2A\_1:3) are characteristic of the  $-\text{OH}$  vibrations in HPMC involved in the formation of the intermolecular H bonds with the PAA polymeric chains.

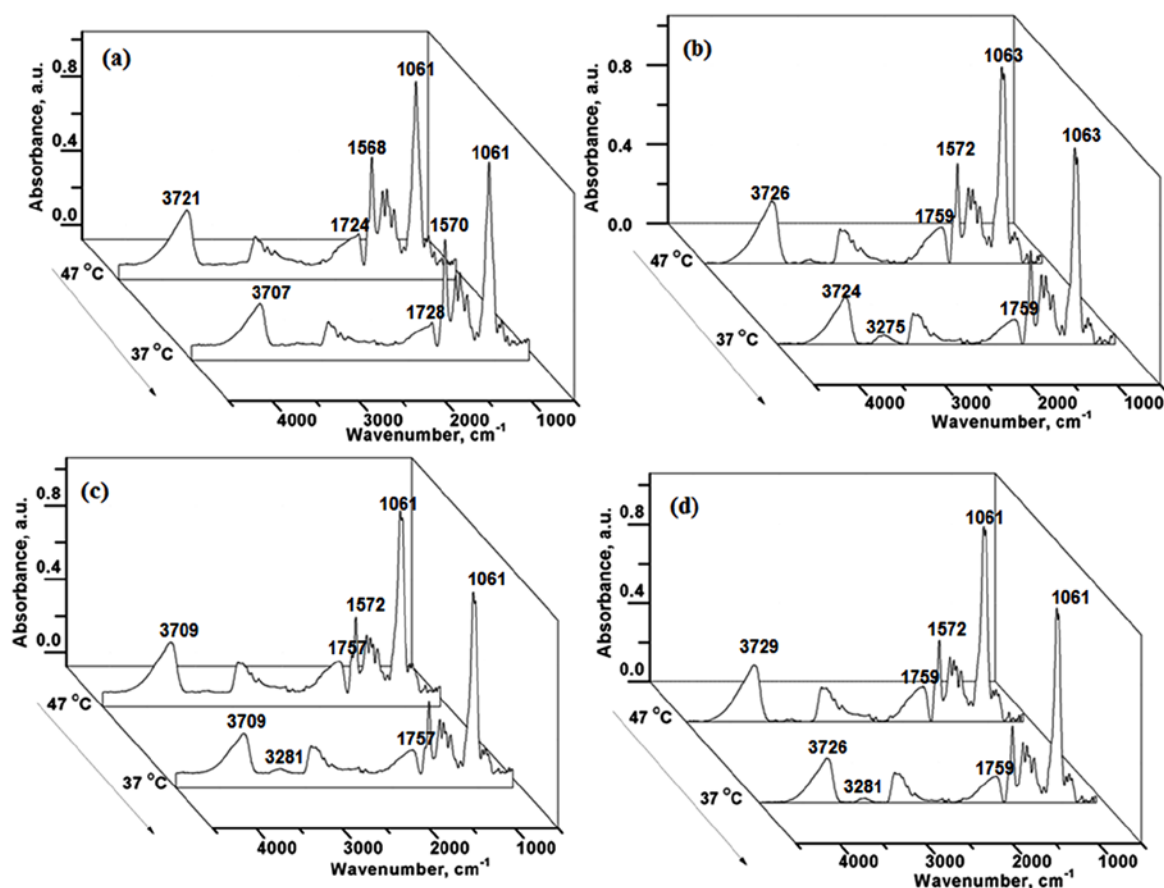


Figure 5: ATR-FTIR spectra of hydrogels F1A (a), F2A (b), F3A (c) and F4A (d) during cooling from 55 to 27 °C

Table 2  
Curve-fitting results of the  $-\text{O}-\text{H}$  spectral region, energy and distances of the hydrogen bonds of the hydrogels under study

Sample	Hydrogen-bonded O-H $\nu$ , $\text{cm}^{-1}$	$E_{\text{H}}$ (kJ)	$R$ ( $\text{\AA}$ )
F1A	3354	21.29	2.773
F1A_1:2	3384	19.13	2.779
F1A_1:3	3380	19.41	2.779
F2A	3334	22.73	2.768
F2A_1:2	3372	19.99	2.777
F2A_1:3	3392	18.55	2.781
F3A	3294	25.60	2.759
F4A	3290	25.89	2.758

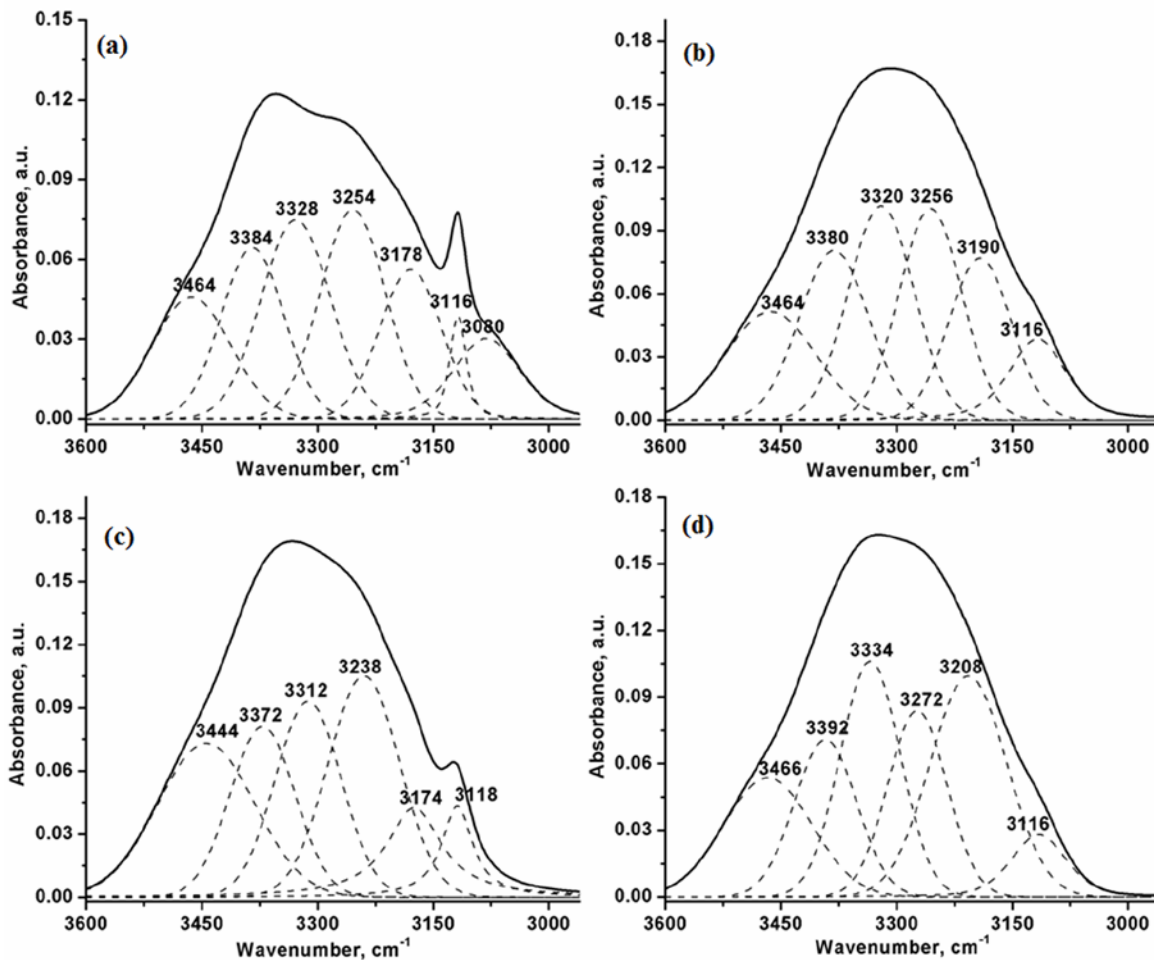


Figure 6: Deconvoluted IR spectra of PAA-HPMC based hydrogels (F1A and F2A) in 2960-3600  $\text{cm}^{-1}$  spectral region: (a) F1A\_1:2, (b) F1A\_1:3, (c) F2A\_1:2, (d) F2A\_1:3

The absorption bands at 3328  $\text{cm}^{-1}$  (F1A\_1:2), 3320  $\text{cm}^{-1}$  (F1A\_1:3), 3312  $\text{cm}^{-1}$  (F2A\_1:2) and 3334  $\text{cm}^{-1}$  (F2A\_1:3) are assigned to the  $-\text{O}\cdots\text{N}$  hydrogen bond interactions between the  $-\text{OH}$  groups of HPMC and the  $\text{C}=\text{N}$  groups of the fluconazole- $\beta$ -CD complex. The  $E_{\text{H}}$  calculated by using the Sederholm equations<sup>13,14</sup> for these interactions was found to be in the range of 11.03-11.64 kJ for F1A\_1:2 and F1A\_1:3, and of 10.57-12.24 kJ for F2A\_1:2 and F2A\_1:3. The absorptions at 3254  $\text{cm}^{-1}$  and 3178  $\text{cm}^{-1}$  (F1A\_1:2), 3256  $\text{cm}^{-1}$  and 3190  $\text{cm}^{-1}$  (F1A\_1:3), 3238  $\text{cm}^{-1}$  and 3174  $\text{cm}^{-1}$  (F2A\_1:2), 3272  $\text{cm}^{-1}$  and 3208  $\text{cm}^{-1}$  (F2A\_1:3) are assigned to the intramolecular H-bonds formed between the  $-\text{OH}$  groups and  $\text{C}-\text{O}-\text{C}$  groups in the structure of HPMC, while the band at 3116  $\text{cm}^{-1}$  is the contribution of the H-bonded  $-\text{OH}$  groups in the PAA polymeric chains and the  $\text{C}-\text{H}$  stretches from the triazole rings (Fig. 6).

The dynamics as a function of temperature of the H-bonds in samples F1A and F2A (Fig. 7 (a), (b)), as well as in F1A\_1:2, F1A\_1:3, F2A\_1:2 and F2A\_1:3 (Fig. 7 (c), (d)), respectively, at 37  $^{\circ}\text{C}$ , revealed the breaking of the H-bonds as the temperature is increased and a higher stability of the gel formulations F2A\_1:2 and F2A\_1:3 at 37  $^{\circ}\text{C}$ . This makes them suitable for applications as drug delivery systems at the physiological temperature of the human body. These systems proved to be sensitive not only to temperature, but also to conditions simulating the physiological environment.<sup>11</sup>

### DSC analysis

DSC offers information on interactions of host-guest type formulations in solid state. The DSC thermograms (first heating run, 10  $^{\circ}\text{C}/\text{min}$ ) of pure fluconazole (FCZ), pure  $\beta$ -cyclodextrin ( $\beta$ -CD), inclusion complexes of FCZ- $\beta$ -CD 1:2 and

FCZ- $\beta$ -CD 1:3 and physical mixture of FCZ and  $\beta$ -CD with 1:2 ratio are shown in Figure 8. Differences between the inclusion complexes and the pure compounds can be remarked during heating due to phase transformations.

In the case of host-guest complexes, a decrease of the melting peak heights of the guest molecule

or the complete disappearance of its melting profile and melting temperature shifts are observed.<sup>27</sup> The pure FCZ molecule exhibits two endothermic transitions at 100 °C and 141 °C, corresponding to dehydration and melting, respectively.<sup>28</sup>

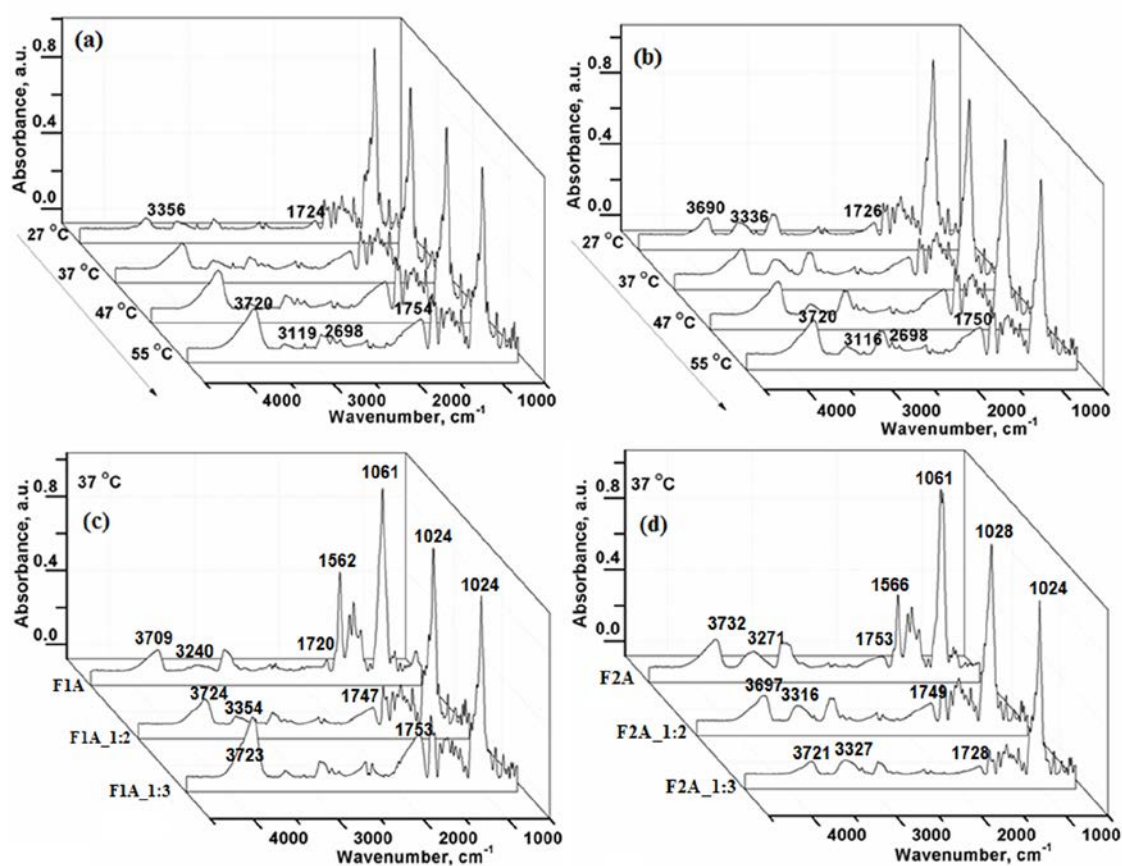


Figure 7: ATR-FTIR spectra of hydrogels F1A (a), F2A (b) during heating from 27 to 55 °C, and comparative behavior of hydrogels F1A, F1A\_1:2 and F1A\_1:3 (c) and F2A, F2A\_1:2 and F2A\_1:3 (d) at 37 °C

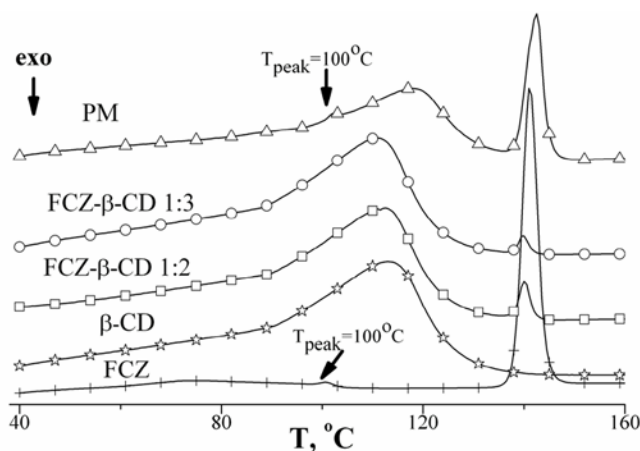


Figure 8: DSC thermograms (first heating run) of the studied compounds

The first heating run of the polymeric matrix also evidences these two transitions. In the case of both host-guest complexes, the dehydration peaks at 100 °C disappear, whereas the heights of the melting peaks of FCZ at around 141 °C decrease with an increasing amount of  $\beta$ -CD in the inclusion complexes and small peak shifts to lower temperatures are observed, due to a new solid phase formation.<sup>29</sup> Pure  $\beta$ -CD exhibits a broad endothermic peak in the temperature range of 90-140 °C caused by loss of crystallized water from its cavity. The dehydration peak temperatures of  $\beta$ -CD slightly shift towards lower temperatures with an increasing amount of  $\beta$ -CD in the complexes. On the basis of melting enthalpy values, the efficiency of loading for the host-guest complexes was evaluated by applying Equation (3):

$$\% \text{Inclusion} = 100 \times \frac{1 - \Delta H_{\text{FCZ-}\beta\text{-CD}}}{\Delta H_{\text{FCZ}}} \quad (3)$$

where  $\Delta H_{\text{FCZ-}\beta\text{-CD}}$  is the melting enthalpy value of the inclusion complex and  $\Delta H_{\text{FCZ}}$  is the melting enthalpy value of pure FCZ. The inclusion efficiency was found higher (96.68%) for FCZ- $\beta$ -CD 1:3 than (92.02%) for FCZ- $\beta$ -CD 1:2.

In Figure 9, the DSC thermograms for the hydrogel formulation containing pure FCZ (F1A\_1) and those with FCZ- $\beta$ -CD 1:2 and FCZ- $\beta$ -CD 1:3 inclusion complexes (F1A\_1:2, F1A\_1:3, F2A\_1:2 and F2A\_1:3) are shown. The values of melting temperatures,  $T_m$ , from DSC (first heating run, 10 °C/min) are tabulated in Table 3. The DSC thermograms reveal multiple endotherms, which can be explained by the fact that the studied hydrogels are multicomponent

systems with complex interactions between constituents.

### TGA

In Figure 10, the TG and DTG curves of pure FCZ, FCZ- $\beta$ -CD 1:2 and FCZ- $\beta$ -CD 1:3 are presented. In Table 4, the thermal characteristics from the thermal decomposition process under nitrogen of pure FCZ, FCZ- $\beta$ -CD 1:2 and FCZ- $\beta$ -CD 1:3 inclusion complexes are presented. The first thermal decomposition stage of each compound corresponds to the dehydration process. The values of moisture content loss from the inclusion complexes, of 10 and 11%, are due to  $\beta$ -CD dehydration. Pure FCZ exhibits a thermal decomposition stage between 230 and 355 °C, reaching a 95% mass loss. By analyzing Figure 10 and Table 4, one may observe that the values of  $T_i$  for the inclusion complexes for the second stage of thermal degradation are higher than that of pure FCZ, indicating a significant increase in the thermal stability of the inclusion complexes. This result is further supported by the higher values of the residue mass for the inclusion complexes than that of pure FCZ.<sup>27</sup>

The amount of  $\beta$ -CD in the inclusion complexes influences the inclusion efficiency in connection with the values of the residue mass and mass loss. Furthermore, the inclusion complexes behave as a single component system, thermally degrading in a single stage, as shown by the DTG curves in Figure 11(b), this also being an indication that a complexation reaction successfully occurred.<sup>30</sup>

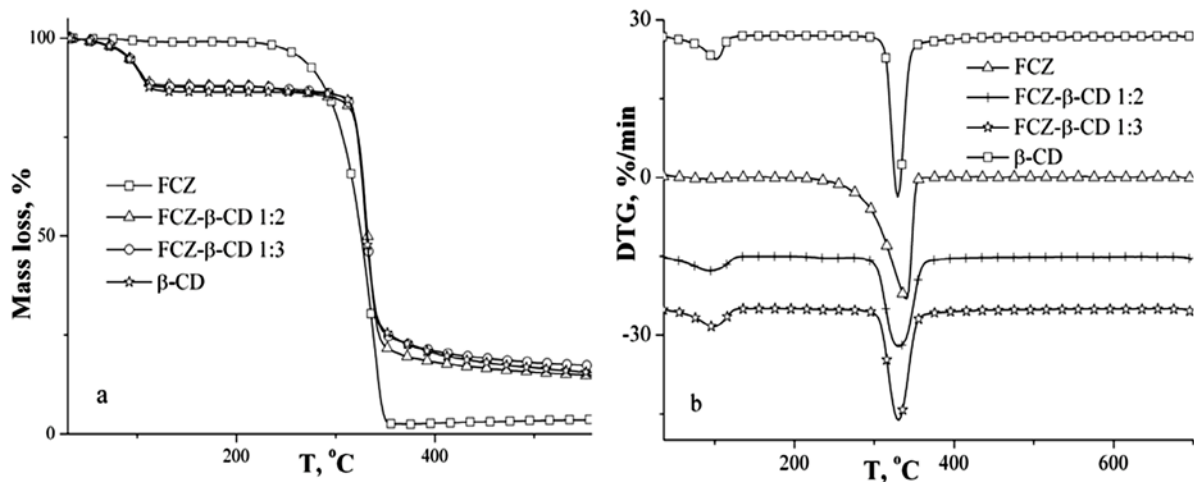


Figure 9: DSC thermograms for hydrogel formulations containing pure FCZ (F1A\_1) and FCZ- $\beta$ -CD 1:2 and FCZ- $\beta$ -CD 1:3 inclusion complexes (F1A\_1:2, F1A\_1:3, F2A\_1:2 and F2A\_1:3)

Table 3  
Thermal characteristics from thermal decomposition under nitrogen and DSC analysis of the studied hydrogel formulations

Sample	Stage	T <sub>i</sub> , °C	T <sub>max</sub> , °C	T <sub>f</sub> , °C	m, %	W, %	T <sub>m</sub> , °C
F1A_1	I	52	76	96	9.6	14.5	97.4
	II	183	222	246	37.7		161.2
	III	246	290	313	26.3		177.6
	IV	354	381	392	10.6		
F1A_1:2	I	51	86	96	5.1	18.4	95.8
	II	189	206	218	13.6		127.7
	III	242	287	314	22.7		181.9
	IV	314	344	356	25		
	V	356	391	417	14.3		
F1A_1:3	I	64	73	107	5.6	13.5	86.4
	II	181	212	226	21		107.1
	III	264	277	285	12.2		171.5
	IV	317	336	351	46		
F2A_1:2	I	53	77	108	6	14.4	95.0
	II	183	214	232	25.5		112.1
	III	257	265	293	14.2		167.6
	IV	319	341	350	23.4		184
	V	350	376	385	15.2		
F2A_1:3	I	60	77	108	6.3	14.3	91.4
	II	184	211	230	16.8		110.5
	III	230	281	292	16.9		172.2
	IV	318	339	357	45		

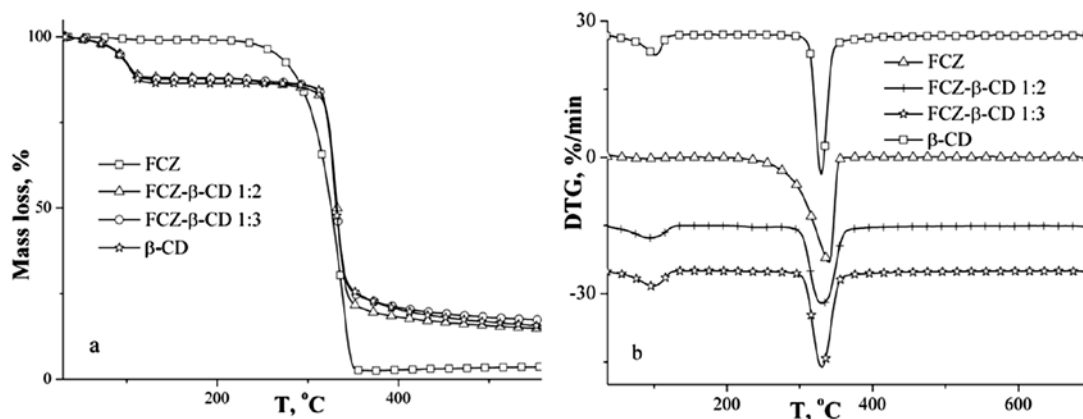


Figure 10: TG (a) and DTG (b) thermogravimetric curves of pure FCZ, FCZ-β-CD 1:2 and FCZ-β-CD 1:3 inclusion complexes

In Figure 11, the TG (a) and DTG (b) thermogravimetric curves of the hydrogel formulations containing pure FCZ (F1A\_1) and FCZ-β-CD 1:2 and FCZ-β-CD 1:3 inclusion complexes (F1A\_1:2, F1A\_1:3, F2A\_1:2 and F2A\_1:3) are presented. In Table 4, the thermal characteristics from the thermal decomposition process under nitrogen and from the DSC analysis of the studied hydrogel formulations are tabulated.

The thermogravimetric curves reveal multiple degradation stages because the studied hydrogels

are multicomponent systems with complex interactions between the constituents. For all the studied hydrogels, stage I of thermal degradation (below 100 °C) corresponds to loss of water. One can notice that the TG/DTG curves of the F1A\_1:2 and F2A\_1:2 samples have a supplementary degradation step (stage V, Table 3). The absence of this last stage in the TG/DTG curves of F1A\_1:3 and F2A\_1:3 samples is explained by an increased content of β-CD in their composition, which stabilizes the polymeric matrix. The TG/DTG profiles for the F1A\_1:2

and F2A\_1:2 samples demonstrate a particular thermal character, compared with the other gel

formulations studied.<sup>31</sup>

Table 4

Thermal characteristics from thermal decomposition process under nitrogen of pure FCZ, FCZ- $\beta$ -CD 1:2 and FCZ- $\beta$ -CD 1:3 inclusion complexes

Sample	Stage	T <sub>i</sub> , °C	T <sub>max</sub> , °C	m, %	T <sub>f</sub> , °C	W, %
FCZ	I	85	90	0.5	110	4
	II	230	340	95	355	
FCZ- $\beta$ -CD 1:2	I	70	100	10	115	13
	II	300	332	72	350	
FCZ- $\beta$ -CD 1:3	I	70	102	11	115	18
	II	300	330	69	350	
$\beta$ -CD	I	33	138	13.5	103	19.7
	II	284	410	66.8	330	

T<sub>i</sub> – initial temperature of thermal decomposition; T<sub>max</sub> – temperature corresponding to the maximum thermal decomposition rate for the first and second stages; T<sub>f</sub> – final thermal decomposition temperature; m – mass loss values corresponding to the first and second thermal decomposition stages; W – residual mass at the end of thermal decomposition (700 °C)

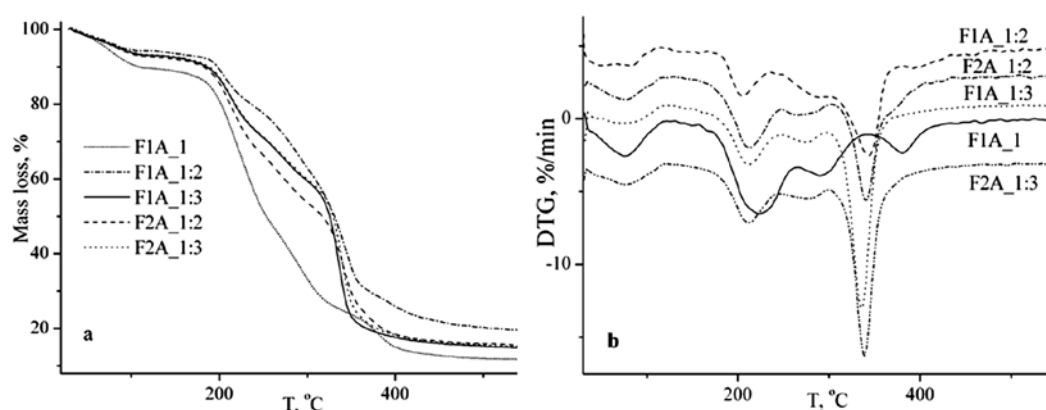


Figure 11: TG (a) and DTG (b) thermogravimetric curves of hydrogel formulations containing pure FCZ (F1A\_1), and FCZ- $\beta$ -CD 1:2 and FCZ- $\beta$ -CD 1:3 inclusion complexes (F1A\_1:2, F1A\_1:3, F2A\_1:2 and F2A\_1:3)

## CONCLUSION

Interpolymer complexes were prepared through hydrogen bonding interactions between HPMC, PAA and anise/fluconazole  $\beta$ -cyclodextrin (FCZ- $\beta$ -CD) inclusion complexes with progressive amounts of HPMC and FCZ- $\beta$ -CD. The formation of strong intermolecular H bonds between HPMC and PAA was evidenced by the shifts of the absorption bands characteristic of the hydroxyl groups in HPMC and PAA in the IR spectra. The H-bonding interactions between HPMC and PAA were found to be stronger upon increasing HPMC content in the mixture, while E<sub>H</sub> varied from 21.29 kJ to 25.89 kJ. This behavior could be due to the complex interactions between the two polymer chains by combining

inter- and intramolecular interactions. The obtained hydrogels were studied by FTIR, in the temperature range of 27-55 °C, in order to evidence the dynamic character of the H bonds. The DSC study evidenced the formation of the FZC- $\beta$ -CD inclusion complex and its successful embedding into the polymeric matrix, while the thermogravimetric curves revealed multiple degradation stages, which are due to the fact that the studied hydrogels are multicomponent systems with complex interactions between the constituents.

**ACKNOWLEDGEMENTS:** This work was supported by a grant of Ministry of Research and Innovation, CNCS - UEFISCDI, project number

PN-III-P1-1.1-PD-2016-1027 (Contract 5/2018), within PNCDI III.

## REFERENCES

- <sup>1</sup> L. Ali, M. Ahmad and M. Usman, *Cellulose Chem. Technol.*, **49**, 143 (2015).
- <sup>2</sup> E. S. M. Negim, Zh. A. Nurpeissova, R. A. Mangazbayeva, J. M. Khatib, C. Williams *et al.*, *Carbohyd. Polym.*, **101**, 415 (2014).
- <sup>3</sup> L.-F. Wang, W. B. Chen, T.-Y. Chen and S.-L. Chun, *J. Biomat. Sci.*, **14**, 27 (2003).
- <sup>4</sup> Y. He, B. Zhu and Y. Inoue, *Prog. Polym. Sci.*, **29**, 1021 (2004).
- <sup>5</sup> C. Spagnol, F. H. A. Rodrigues, A. G. B. Pereira, A. R. Fajardo, A. F. Rubira *et al.*, *Carbohyd. Polym.*, **87**, 2038 (2012).
- <sup>6</sup> K. Sudarsan Reddya, M. N. Prabhakara, K. Madhusudana Raob, D. M. Suhasinib, V. Naga Maheswara *et al.*, *Indian J. Adv. Chem. Sci.*, **2**, 38 (2013).
- <sup>7</sup> M. M. Coleman and P. C. Painter, *Prog. Polym. Sci.*, **20**, 1 (1995).
- <sup>8</sup> T. Kondo, C. Sawatari, R. S. J. Manley and D. G. Gray, *Macromolecules*, **27**, 210 (1994).
- <sup>9</sup> T. Kondo and C. Sawatari, *Polymer*, **35**, 4423 (1994).
- <sup>10</sup> C. A. Gafitanu, D. Filip, C. Cernatescu, C. Ibanescu, M. Danu *et al.*, *Biomed. Pharmacother.*, **83**, 485 (2016).
- <sup>11</sup> C. A. Gafitanu, D. Filip, C. Cernatescu, D. Rusu, C. G. Tuchilus *et al.*, *Pharm. Res.*, **34**, 2185 (2017).
- <sup>12</sup> J. Lawless, "The Encyclopedia of Essential Oils", Conari Press, 2013, pp. 38-39.
- <sup>13</sup> G. C. Pimentel and C. H. Sederholm, *J. Chem. Phys.*, **24**, 639 (1956).
- <sup>14</sup> H. Struszczyk, *J. Macromol. Sci.*, **23**, 973 (1986).
- <sup>15</sup> C. Djahedi, M. Bergenstrahle-Wohlert, L. A. Berglund and J. Wohlert, *Cellulose*, **19**, 1821 (2012).
- <sup>16</sup> R. G. Zbankov, *J. Mol. Struct.*, **270**, 523 (1992).
- <sup>17</sup> M. Fan, D. Dai and B. Huang, in "Fourier Transform – Materials Analysis", edited by S. Salih, InTech, 2012, pp. 45-68.
- <sup>18</sup> S. Spoljaric, A. Salminen, N. D. Luong and J. Seppala, *Cellulose*, **20**, 2991 (2013).
- <sup>19</sup> E. S. M. Negim, Zh. A. Nurpeissova, R. A. Mangazbayeva, J. M. Khatib, C. Williams *et al.*, *Carbohyd. Polym.*, **101**, 415 (2014).
- <sup>20</sup> M. Zigon and G. Ambrozic, *Materiali tehnologije*, **37**, 231 (2003).
- <sup>21</sup> M. F. Zaltariov, M. Cazacu, S. Shova, A. Vlad, I. Stoica *et al.*, *J. Pol. Sci. A. Chem.*, **50**, 3775 (2012).
- <sup>22</sup> A. R. H. Cole, "Tables of Wavenumbers for the Calibration of Infrared Spectrometers", second edition, University of Western Australia, Pergamon Press, 1977, p. 21.
- <sup>23</sup> T. Pinault, B. Andrioletti and L. Bouteiller, *Beilstein J. Org. Chem.*, **6**, 869 (2010).
- <sup>24</sup> G. Yurtdas, M. Demirel and L. Genc, *Incl. Phenom. Macrocycl. Chem.*, **70**, 429 (2011).
- <sup>25</sup> X. J. Gu and W. Jiang, *J. Pharm. Sci.*, **84**, 1438 (1995).
- <sup>26</sup> D. Lin-Vien, N. B. Colthup, W. G. Fateley and J. G. Graselli, "The Handbook of Infrared and Raman Characteristic Frequencies of Organic Molecules", Academic Press, Boston, 1991, pp. 117-261.
- <sup>27</sup> N. Marangoci, M. Mares, M. Sillion, A. Fifere, C. Varganici *et al.*, *Res. Pharm. Sci.*, **1**, 27 (2011).
- <sup>28</sup> M. Lemsı, M. R. Louhaichi, H. Galai, M. C. Benrayana and R. Kalfat, *J. Chem. Pharm. Res.*, **5**, 950 (2013).
- <sup>29</sup> A. Corciova, C. Ciobanu, A. Poiata, C. Mircea, A. Nicolescu *et al.*, *Incl. Phenom. Macrocycl. Chem.*, **81**, 71 (2015).
- <sup>30</sup> C.-D. Varganici, N. Marangoci, L. Rosu, C. Barbu-Mic, D. Rosu *et al.*, *J. Anal. Appl. Pyrol.*, **115**, 132 (2015).
- <sup>31</sup> Y. Liu, L. Li, G. Dong, Y. Yang, C. Zheng *et al.*, *Cellulose Chem. Technol.*, **50**, 897 (2016).